J. Appl. Cryst. (1997). **30**, 280–293

The Time-of-Flight Small-Angle Neutron Diffractometer (SAD) at IPNS, Argonne National Laboratory

P. THIYAGARAJAN,* J. E. EPPERSON,† R. K. CRAWFORD, J. M. CARPENTER, T. E. KLIPPERT‡ AND D. G. WOZNIAK

Intense Pulsed Neutron Source Division, Argonne National Laboratory, 9700 South Cass Avenue, Argonne, IL 60439, USA. E-mail: thiyaga@anlpns.pns.anl.gov

(*Received 12 April 1996; accepted 24 October 1996*)

Abstract

The design, development and performance of the time-of-flight (TOF) small-angle diffractometer (SAD) at the Intense Pulsed Neutron Source (IPNS) at Argonne National Laboratory are described. Similar TOF-SANS instruments are in operation at the pulsed neutron sources at Los Alamos National Laboratory, USA, at Rutherford Appleton Laboratory, England, and at KEK, Japan. These instruments have an advantage by comparison with their steady-state counterparts in that a relatively wide range of momentum transfer (q) can be monitored in a single experiment without the need to alter the collimation or the sample-to-detector distance. This feature makes SANS experiments easy and very effective for studying systems such as those undergoing phase transitions under different conditions, samples that cannot be easily reproduced for repetitive experiments, and systems under high temperature, pressure or shear. Three standard samples are used to demonstrate that the quality of the SANS data from SAD is comparable with those from other established steady-state SANS facilities. Two examples are given to illustrate that the wide q region accessible in a single measurement at SAD is very effective for following the time-dependent phase transitions in paraffins and temperature- and pressure-dependent phase transitions in model biomembranes.

1. Introduction

SANS is a nondestructive technique which can provide information on the size, shape, volume fraction and interactions of particles whose size falls in the range of ten to a few thousand ångströms. SANS can readily be applied to study amorphous and solution samples and has been very effective for studying the organization of molecules in supramolecular structures in biological and other self-assembling materials, phase transitions and kinetic phenomena in biology, polymers, metallic alloys, micelles, ceramics, microemulsions, magnetic systems *etc.* (Guinier & Fournet, 1955; Jacrot, 1976; Kostorz, 1979; Wignall, 1987; Chen, 1986). The high penetration of neutrons makes them particularly valuable for studying bulk solid and liquid samples.

Tremendous growth in SANS applications has occurred following the development of instruments at the reactor sources (Ibel, 1976; Koehler, 1986). Cold moderators such as liquid hydrogen and liquid deuterium enhance the flux at long wavelengths and consequently enable the acquisition of high-quality data in the very low q region ($q = 4\pi \sin\theta/\lambda$, where θ is half the scattering angle and λ is the wavelength). In order to maximize the information about any small-angle scattering experiment, it is necessary that the data be available in a wide q region. Data in a wide q range can be easily obtained in a single measurement from the pulsed-source based time-of-flight SANS (TOF-SANS) instruments which use a fixed geometry but utilize neutrons with a wide range of wavelengths. At the reactor-based instruments (steady state) the data in a wide q range are obtained by repetitive measurements on the sample using several reconfigurations of the instrument (altering collimation-to-sample and sample-to-detector distances). This works well for stable samples that do not undergo any variation during the intermediate times of storage and handling between measurements. However, this becomes a drawback for the study of systems that may slowly alter over time (*e.g.* complexes of biopolymers in equilibrium with subunits) or systems that cannot be accurately reproduced for the repetitive experiments.

TOF-SANS instruments are currently in use at the IPNS at Argonne National Laboratory and five other laboratories in the world. Among these are the instruments at the other pulsed spallation neutron sources at Los Alamos National Laboratory in the USA (Seeger, Hjelm & Nutter, 1990), at the Laboratory for High Energy Physics (KEK) in Japan (Ishikawa, Furusaka, Nimura, Arai & Hasegawa, 1986) and at the Rutherford Appleton Laboratory in UK (Heenan & King, 1993). A TOF-SANS instrument is in operation at the pulsed

† APS Division.
‡ Material Science Division, retired.

reactor IBR-2 at the Joint Institute for Nuclear Research at Dubna in Russia (Ostanevich, 1988). Time-of-flight techniques with choppers were used on a reactor-based SANS instrument at CEN, Saclay, France (Cotton & Teixiera, 1986).

Development of the pulsed source TOF-SANS capabilities began at Argonne National Laboratory in 1979. At the time the development of TOF-SANS instruments began, there was no generally agreed upon design; hence, their development has been, and continues at this date to be, an evolutionary process. Contrary to early skepticism, pulsed neutron sources equipped with cold moderators have proved to be quite suitable for SANS applications. The purpose of this contribution is to describe the various components of the currently operating small-angle diffractometer (SAD) at IPNS, to relate the experience with its development, and to demonstrate that the quality of the data from SAD is quite similar to those from the established SANS facilities and that the SAD is powerful for time-dependent SANS studies on systems undergoing phase transitions.

2. Instrument design and components

The SAD is a short flight-path TOF-SANS instrument situated on beamline C1 at IPNS. Fig. 1 shows the schematic and Table 1 collects all the relevant parameters of this instrument. Briefly, neutrons from a pulsed spallation source are thermalized by a cryogenic moderator suitable for SANS investigations. A crossed pair of Soller collimators focuses the neutron beam at an area-sensitive gas-filled proportional counter which measures the scattered neutrons. Details of the components of SAD are described below.

2.1. *Target and moderator*

Neutrons in pulses (30 Hz) are produced at IPNS by spallation in a uranium target by 450 MeV proton pulses (0.3 μs duration) with a time-averaged proton current of 15 μA. Both depleted uranium ^{238}U and uranium 77.5% enriched in ^{235}U targets were used. Since the neutrons produced by spallation have very high energy, they are not useful for the low-q applications and hence have to be thermalized. The moderators for TOF-SANS applications at the short pulsed neutron sources are designed such that sufficient flux of thermal neutrons is produced with a narrow pulse width at the moderator (Carpenter & Yelon, 1986). SAD has used a moderator with either liquid hydrogen at 20 K or solid methane at 28 K, in a 0.7 l aluminium container which is grooved on the viewed side to increase the cold neutron flux. The moderator is surrounded by graphite and beryllium as reflector, decoupled by a 0.5 mm layer of cadmium. The use of solid methane in place of liquid hydrogen in this moderator enhances the long-wavelength neutron flux by over threefold as depicted in Fig. 2. The pulse width

Table 1. *Parameters for SAD*

Parameter	Value
Source frequency	30 Hz
Moderator	Decoupled solid CH_4
Source-to-sample distance	7.583 m
Source-to-beam monitor (M_1)	6.313 m
Source-to-transmitted beam monitor (M_2)	8.643 m
Sample-to-area detector distance	1.504 m
Focusing collimators	0.0034 rad FWHM
Vertical focusing collimator	
Entrance width/channel	0.0974 cm
Exit width/channel	0.0851 cm
Collimator exit–sample distance	32.8 cm
Length	75 cm
Horizontal focusing collimator	
Entrance width/channel	0.0844 cm
Exit width/channel	0.0750 cm
Collimator exit–sample distance	25 cm
Length	50 cm
Beam diameter at moderator	9.0 cm
Beam diameter at area detector	2.1 cm
Area detector	
Active volume	20 × 20 cm, 3.2 cm thick
Resolution	6–8 mm FWHM
Wavelength range	0.9–14 Å
q range (single experiment)	0.005–0.35 $Å^{-1}$

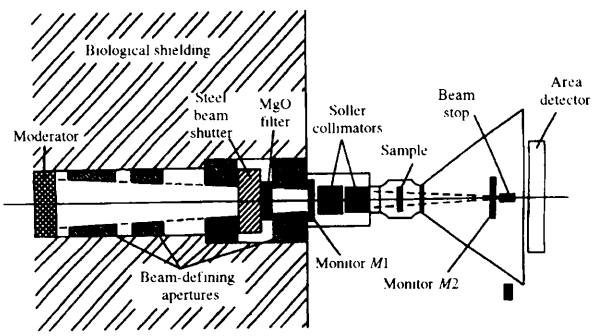

Fig. 1. Schematic representation of the SAD. See Table 1 for all the relevant instrument parameters.

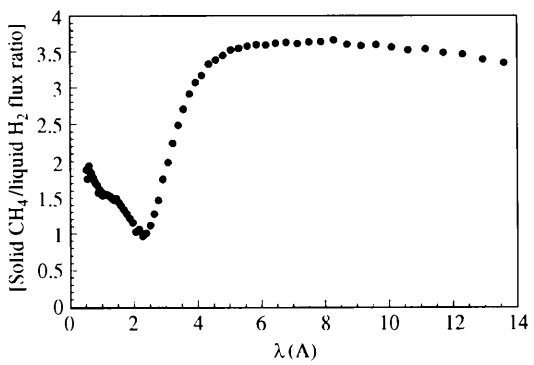

Fig. 2. Ratio of neutron flux from a solid methane moderator at 28 K and that from a liquid-hydrogen moderator at 20 K. The solid methane moderator provides about three fold increase in the neutron flux in the long-wavelength region.

for 1 Å neutrons is ~ 15 μs and it increases with increasing wavelength, reaching a value of ~ 300 μs for 14 Å neutrons. It should be noted that the magnitude of the pulse width is too small to cause any significant effects on the q resolution of SAD. The solid methane moderator, however, is subject to occasional uncontrolled temperature increases ('burps') in which the products of radioalysis, stored as chemical energy, are released rapidly and spontaneously, on occasion even rupturing the aluminium container (Carpenter, Walter & Mildner, 1986; Carpenter, 1987). Recently, a procedure has been developed in which controlled burping at specific time intervals is carried out by slow increasing of the temperature of the moderator to ~ 90 K to release the stored energy and cooling back to 28 K.

2.2. *MgO single-crystal filter*

The spectrum of prompt neutrons from the solid methane moderator viewed by SAD contains a significant amount of fast neutrons and γ-rays that introduce deleterious detector recovery effects which can persist to long times-of-flight. These have to be attenuated for SANS applications. Currently, three different techniques are in use to reduce or eliminate the fast neutrons at different pulsed neutron sources. The SANS instrument at the KENS pulsed source at KEK in Japan uses a long reflecting bent neutron guide to make the detector out of sight of the source (Ishikawa *et al.*, 1986). The disadvantage of this method is that the longer flight path restricts the maximum wavelength up to which measurements can be made (frame-overlap constraint). The LOQ instrument at the ISIS pulsed source in England (Heenan & King, 1993), on the other hand, employs a beam bender (an array of short narrow curved guides placed side by side) for this purpose. However, this cuts off neutrons with wavelengths below 2 Å, limiting measurements in the high-q region. A third method is to insert a filter made of a crystalline material that can eliminate short-wavelength neutrons by Bragg diffraction and/or inelastic scattering. SAD at IPNS and LQD at LANSCE use liquid-nitrogen-cooled single-crystal MgO filters for reducing the fast neutrons. The downside of using a filter is that it can also attenuate the useful long-wavelength neutron flux. Hence, it is essential to optimize its design such that it is very effective in attenuating the fast neutrons, but causes the least attenuation of the useful long-wavelength neutrons. Cooling the MgO filter from room temperature to 77 K enhances the transmission factors for the long-wavelength neutrons by almost a factor of two. The neutron spectrum measured by the incident-beam monitor (M_1) at SAD after the neutron beam passes through a cold MgO filter at 77 K is shown in Fig. 3. The dip in the intensity distribution at $\lambda = 4$ Å in Fig. 3 is due to the Bragg scattering from the aluminium vacuum window. The measured transmission factors in the cold MgO filter as a function of neutron wavelength are shown in Fig. 4. The net transmission of cold MgO filter at SAD is $\sim 70\%$ in the long-wavelength region. On the short-wavelength side, the transmission factors start to decrease at $\lambda \simeq 1.5$ Å and quickly reach a value of $\sim 10\%$ for neutrons with $\lambda \simeq 0.5$ Å. Below this wavelength, the transmission factor continues to decrease with decreasing wavelength (data not shown).

Fig. 5 shows a higher-resolution spectrum from M_1 for the short-wavelength region of the spectrum. The dips designated as 1, 2 and 3 correspond to Bragg spacings of 2.10, 1.68 and 1.40 Å, respectively (Carpenter, Mildner, Cudrnat & Hilleke, 1989), and these are used for measuring the distances of the monitors, the area detector and the sample (with a monitor detector temporarily placed at this location) from the source by the relationship.

$$L_i = ht_i/m\lambda_j, \tag{1}$$

where h is Planck's constant, m is the neutron mass, t_i is the mean flight time to detector i, λ_j is the wavelength of the neutrons corresponding to the d-spacing for the line j, being used as the 'tag', and L_i is the distance from the source to the ith detector. With this procedure, we are assured that the TOF-to-wavelength calibrations at different detectors are matched.

2.3. *Collimation*

The SAD instrument uses a multiple-aperture collimator consisting of a crossed pair of converging Soller collimators, one for vertical definition and the other for horizontal definition of the angular distribution (Fig. 6). The Soller elements were fabricated by CIDIC Ltd. (Cirencester Rd, Cheltenham, England); their performance characteristics and method of production have been described by Carlile, Hey & Williams (1977) and Carlile, Penford & Williams (1978). Each element focuses the neutron beam on the detector plane ~ 2 m from the collimator exit. Each element contains 22 vanes consisting of aluminized Mylar stretched over tapered steel frames and coated with a ^{10}B-containing

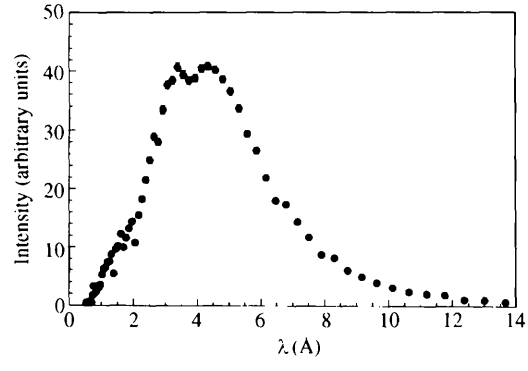

Fig. 3. Spectral distribution as a function of neutron wavelength at SAD.

paint, whose high absorption cross section prevents cross-talk between channels for wavelengths down to at least 0.1 Å. This use of focused multi-aperture collimators achieves the necessary angular collimation without sacrificing the flux on the sample or the q resolution, while still maintaining the lowest possible q (Nunes, 1974, 1978; Carpenter & Faber, 1978). The minimum scattering angle θ_{min} is determined by the penumbra of the beam at the detector and by the spatial resolution of the area detector. That is,

$$2\theta_{min} \simeq (W_p + W_d)/2L_2, \qquad (2)$$

where L_2 is the distance between the sample and the detector, W_p is the maximum penumbra width (2.1 cm for SAD) and W_d is the FWHM resolution of the detector element. The detector resolution function is roughly Gaussian, so FWHM gives a reasonable width estimate. For both collimators of SAD, $\theta_{min} \simeq 0.26°$. However, a beam stop in front of the detector, having a radius of 1.25 cm, makes $\theta_{min} = 0.308°$ so that $q_{min} = 0.067/\lambda_{max}$.

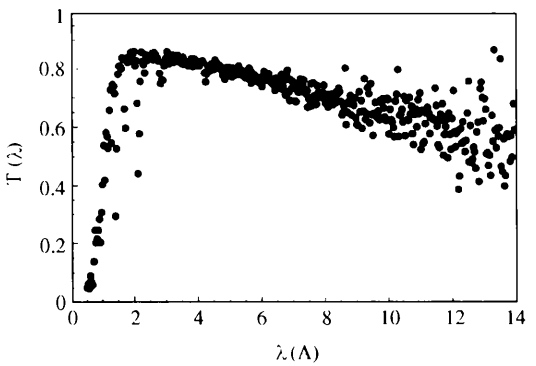

Fig. 4. Wavelength-dependent transmission factors for the liquid-nitrogen-cooled MgO single-crystal filter.

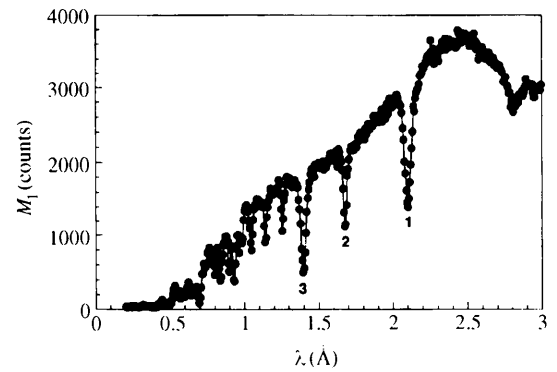

Fig. 5. The neutron spectrum after passing thorough the cold MgO filter. The negative peaks due to Bragg scattering by the MgO single crystal are used for calibrating the distances at SAD. The lines marked 1, 2, 3 correspond to Bragg reflections of 2.10, 1.68 and 1.40 Å, respectively.

The first set of Soller collimators used at SAD produced an anisotropic background. This background was troublesome, especially when anisotropic and weak scatterers were investigated. The anisotropic background was due to the reflections of neutrons by the smooth surfaces of the vanes of these Soller elements (Crawford, Epperson & Thiyagarajan, 1989). During the past eight years, SAD has used Soller elements with somewhat rougher surfaces (matte finish) produced by CIDIC, and with these the anisotropic background lies below the measurement threshold.

2.4. *Detectors*

The detection system of SAD consists of an incident-beam monitor (M_1), a transmitted-beam monitor (M_2), a protons-on-target counter and a position-sensitive area detector. The characteristics of these are described below.

2.4.1. *Incident-beam monitor (M_1).* The incident-beam monitor is a low-efficiency transmission detector which continuously measures the incident beam to provide the integrated intensity as a function of time slice (wavelength of the neutrons). Because the beam is transmitted through this detector, it should have high transmission factors and low efficiency, and must produce the least perturbation of the incident beam.

The detector which performed well and provided a long-term stability during the past ten years is a commercial, planar, pulsed-ion chamber (Reuter-Stokes model RS-P1-3402-101: Reuter-Stokes, Twinsburg, OH, USA), 7.6 cm diameter × 2.5 cm thick, having aluminium walls and containing a low partial pressure of BF_3 as the neutron absorber in the P-10 (mixture of methane, argon and CO_2) fill gas. The BF_3 content of this detector gives an efficiency of $\sim 10^{-3}$ for 1 Å neutrons, with efficiency increasing linearly with wavelength.

Initially, SAD used a commercial charged-particle detector (Ortec Series A Si surface-barrier detector: EG&G Ortec, Oak Ridge, TN, USA), which had ^{6}Li

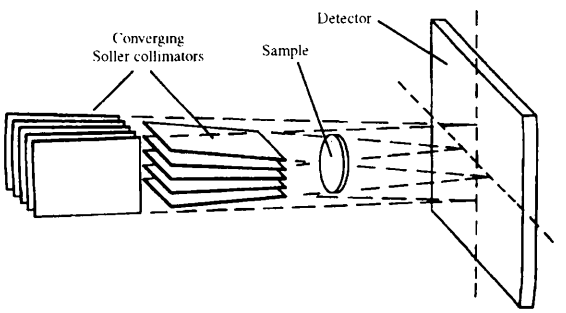

Fig. 6. Schematic of vertical and horizontal focusing arrays of Soller collimators used at SAD.

vapor deposited onto a Si surface, and the following principle was used for detection:

$$^6\mathrm{Li} + \mathrm{n} \rightarrow {}^3\mathrm{H} + {}^4\mathrm{He} + 4.79\ \mathrm{MeV}. \qquad (3)$$

The detection efficiency for a deposition density of 9.5 μg cm^{-2} of ^{6}Li layer was $\sim 5 \times 10^{-4}$ for 1 Å neutrons, that increased linearly with wavelength. The thin single crystal of high-purity Si (resistivity 6.0 kΩ cm) that formed the bulk of the detector produced little neutron absorption or scattering in the wavelength range of interest. We have used two detectors of this kind that worked well initially, but over a period of one year they degraded owing to radiation damage.

2.4.2. *Transmitted-beam monitor (M_2).* A 2.5 cm diameter × 20 cm long cylindrical gas proportional counter containing BF_3 as the neutron absorber is used as a transmitted-beam monitor which is at a distance of 1.06 m from the sample position. On this detector, a 2.25 cm-diameter cadmium mask has been mounted to restrict the solid angle of neutron detection to a circle centred on the direct beam. This ensures that most of the sample small-angle scattering outside the direct-beam penumbra is excluded from the transmission measurements. This is very important for measuring transmission factors for very strong scatterers such as systems showing critical phenomena. The aperture is slightly larger than the penumbra to facilitate alignment of the M_2 monitor and mask. The detector is mounted on a computer-interfaced translation stage so it can be automatically inserted into the beam when desired, and retracted for the scattering measurements. The performance of this detector has been satisfactory over ten years.

2.4.3 *Protons-on-target counter.* The data-acquisition system includes a counter to determine the number of protons produced during the actual measurement. This information is calculated by integration of a train of standard pulses generated from a toroidal detector sensing the proton beams hitting the target. This counter serves two purposes: (i) to determine the integrated beam current used in a given experiment, and (ii) to monitor the performance of the MgO filter and the moderator by using the count rates of the M_1 monitor as a reference.

2.4.4 *Area detector.* SAD employs an area-sensitive gas proportional counter, with an active volume of 20 × 20 × 3.2 cm filled with a mixture of 65% ^{3}He and 35% CF_4 to a total pressure of 0.2 MPa. The anode plane is in the center, sandwiched between front and rear single-wire cathode planes which produce the x and y signals. The cathode wires are strung in a zigzag pattern with 2 mm spacing, with the wire directions in the front plane being orthogonal to those in the rear. Rise-time encoding (Borkowski & Kopp, 1975) utilizing a direct-time-digitizer (Lynch, 1980) produces digital x and y positions encoded with 8 bits each. The intrinsic RC time-constant for each cathode is ~0.8 μs. Pulse-height discrimination is used to eliminate events due to γ-rays and fast neutrons. The position resolution of this detector is 7.5 mm (FWHM) when operated with amplifier time constant sufficiently long to produce good encoding linearity. During the past two years, we have observed degradation of an area detector using the ^{3}He and CF_4 gas mixture in which the sensitivity of pixels in the region of the most intense scattered beam progressively decreases with exposure time. Test experiments show that the degradation is actually due to the interactions involving the CF_4, so alternative fill gases (*e.g.* Xe) are being explored.

2.5. *Data-collection system*

A Vaxstation (Digital Equipment Corporation, Maynard, MA, USA) operates as a general user interface for SAD. The digitized signals from the direct-time-digitizer are initially stored, along with an encoded neutron flight time (TOF), in a buffer in a CAMAC module in a standard IPNS front-end data-acquisition system (Crawford *et al.*, 1981; Haumann, Daly, Worlton & Crawford, 1982; Felcher *et al.*, 1987). Another CAMAC module in the data-acquisition system discriminates and time-encodes the pulses from the upstream and transmission monitors and stores the events in its own buffer. A multiple-microprocessor system (Haumann & Crawford, 1987) sorts out the data from these buffer regions to form TOF histograms for the beam monitor and an x–y–time histogram for the area detector. These histograms are formed in the microprocessor system memory which allows up to 8 Mbytes of histogram space. The histogramming is table-driven and is under complete software control, so it is possible to select individually the range of TOF values to be included in each time slice in the area-detector histogram and to select individually the range of x and y values to be included in each bin within that slice. Normal operation for this instrument involves using N time slices of equal time width (constant Δt bins) or N slices having time-widths proportional to time (constant $\Delta t/t$ bins), and combining all events having encoded x, y values that lie within a 4 × 4 pixel region into the same bin within a slice. This produces an x–y–t histogram of size 64 × 64 × N, where N is typically 67 for a constant $\Delta t/t = 0.05$. Other histogramming combinations are used for testing, calibration and special purposes.

2.6. *Sample environment*

SAD operates mainly on the basis of proposals that are reviewed for scientific merit by the IPNS Program Advisory Committee, which consists mostly of scientists

Table 2. *Ancillary equipment at SAD*

Equipment	Environment	Condition
Sample changer (seven positions)		
Circulating bath	Air	273–348 K
Biological well		
Circulating bath	Air	268–423 K
Resistance heater	Air	Ambient to 473 K
Pressure cell	Hydrostatic pressure	273–353 K 0.1–250 MPa
Rotators for slurries	Air	Ambient
Stretcher for polymers	Air	Ambient
Displex	High vacuum	20–300 K
Metallurgical configuration		
Furnace tube	Vacuum	Ambient
Furnace in a ceramic tube	He purge	373–1473 K
Electromagnet	Air	0.5 T (2 in between poles) 1 T (1 in between poles)
Electromagnet and furnace	He purge	293–1023 K
Electromagnet and displex	High vacuum	20 to 300 K

from outside Argonne National Laboratory. Metallurgists, solution chemists, biologists, polymer scientists and solid-state physicists use this instrument. Consequently, capabilities for a range of sample environments are provided (see Table 2). The temperature controllers for the various furnaces and for the Displex refrigerator are under computer control.

3. Data reduction

In the case of TOF-SANS instruments, neutrons with a broad distribution of wavelengths are binned into several time channels and the scattered neutrons in each time channel are recorded separately by an area detector with several position channels. Thus, neutrons in a time channel t_k arriving at the (i,j)th detector element will have a nominal q value whose magnitude is given by

$$q_{i,j,k} = (m/h)(L/t_k)4\pi \sin\theta_{i,j}, \tag{4}$$

where m is the neutron mass, h is Planck's constant, L is the total source-to-detector distance and θ_{ij} is half the scattering angle at the center of the (i,j)th detector element. Since neutrons recorded in different (i,j,k) cells may have similar values of q, the data in these cells can be combined into bins with a central q value and a finite width.

The area detector at SAD covers a range of scattering angles from $2\theta \simeq 0.57$ to $2\theta \simeq 3.7$ or $2\theta \simeq 5.7°$ (depending on whether the detector is located on-center or off-center with respect to the main beam). The q range accessed by the TOF-SANS instrument depends on the range of scattering angle and the range of wavelength,

$$q_{\min} = 4\pi \sin\theta_{\min}/\lambda_{\max}, \tag{5}$$

$$q_{\max} = 4\pi \sin\theta_{\max}/\lambda_{\min}. \tag{6}$$

Fig. 7 shows the q range spanned by selected wavelengths at SAD. Normally, the data from $\lambda > 0.9$ Å only are used because of the low flux below that wavelength (see Fig. 3) and the data are binned only in the interval $0.005 < q < 0.35$ Å^{-1}, since both the statistical precision and the Δq resolution deteriorate in the high-q region. Depending on the resolution requirement, users can also alter the binning parameters during the data-reduction stage.

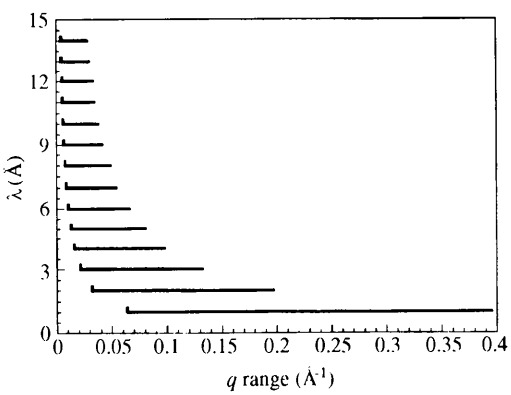

Fig. 7. The q range at selected neutron wavelengths at SAD. The q range at each wavelength is determined by the scattering angle range ($2\theta \simeq 0.57$–$3.7°$) subtended by the area detector.

3.1. *Corrected scattering intensity*

The net scattering intensity for a sample is calculated according to the relationship

$$\begin{aligned} S(i,j,k) = \{&[1/T_s(k)][I_s(i,j,k)/M_{1s}(k) \\ &- I_c(i,j,k)/M_{1c}(k)] \\ &- [1/T_b(k)][I_b(i,j,k)/M_{1b}(k) \\ &- I_c(i,j,k)/M_{1c}(k)]\}/\eta(i,j)\xi(k). \end{aligned} \quad (7)$$

This equation requires the measured raw scattering data for the sample, $I_s(i,j,k)$, its corresponding background, $I_b(i,j,k)$, the blocked-beam background measured with cadmium in the beam, $I_c(i,j,k)$, data on the wavelength-dependent transmission coefficients for the sample, $T_s(k)$, and its corresponding background, $T_b(k)$, the wavelength-dependent efficiency ratio between the area detector and the M_1 monitor, $\xi(k)$, and the detector sensitivity of the pixels in the area detector, $\eta(i,j)$. M_s, M_b and M_c in (7) are the counts on monitor M_1 corresponding to the sample, background and cadmium, respectively, during the scattering measurements, and i,j,k refer to the x,y and TOF coordinates of the data. The wavelength of the neutrons for a given kth bin is calculated using its mean value of the time-of-flight and (1). To determine the position coordinates of the individual pixels (i,j) of the area detector, flood patterns are measured with a 20 × 20 cm boron nitride mask using the neutrons from a Pu–Be source enclosed in a 30 cm-thick block of paraffin for moderation. The thickness of the boron nitride mask is 2 cm and there are 56 1 cm-diameter holes distributed at regular intervals across the whole area. Two-dimensional least-squares fitting of the actual coordinates of the holes in the mask and the measured encoded coordinates of the peaks corresponding to the holes is done to identify the non-linear regions, as well as to determine the channel widths of individual pixels (i,j) in the linear region and the resolution across the detector (Thiyagarajan *et al.*, 1992; Crawford *et al.*, 1994). The scattering angles subtended by the area-detector pixels (i,j) are determined from the distance of the pixels from the beam center and the sample-to-detector distance. $S(i,j,k)$ is then expressed as $S(\theta,\lambda)$ and sorted into an $S(q)$ array either in constant Δq intervals or in variable Δq intervals consistent with the resolution of the instrument.

3.2. *Sensitivity of detector pixels*

The sensitivity of the detector is not perfectly uniform over its active area and has to be accounted for in the data treatment. Only the relative variation in the sensitivity across the detector is required and this can be measured by using either the neutrons from the accelerator or the moderated neutrons from a portable Pu–Be source. The incoherent scattering from either a 1 mm water sample or a 2–3 mm-thick vanadium sample can be measured by using the neutrons from the accelerator. This, in principle, will provide information on both the sensitivity of the pixels in the area detector and the spectral distribution of the neutrons. Although this works extremely well at the high-flux steady-state SANS instruments, this is not practical at the pulsed-source instruments. The reasons are (i) the neutron flux in the most important long-wavelength region is so very low that high-quality sensitivity data as a function of neutron wavelength cannot be obtained in that region without the investment of an enormous amount of beam time, and (ii) the scattering cross sections for water in the region of wavelengths used at SAD are not accurately known. Furthermore, it has been clearly shown that a 1 mm water sample is not useful for detector normalization and calibration at the pulsed-source SANS instruments as the calibration is effectively made with neutrons at wavelengths that may be very different to those in the incident beam (Ghosh & Rennie, 1990; Rennie & Heenan, 1993). Hence, at SAD, the sensitivity of the pixels is measured using the moderated neutrons from a Pu–Be source. Despite the fact that the energy spectrum of the neutrons from the Pu–Be source is quite different from that from the cold source, this procedure is still valid for measurement of the relative sensitivities of the detector pixels. The flood-pattern data of the area detector $A(i,j)$ are always measured when the accelerator is not in operation. The relative sensitivity for a given spatial element (i,j) is defined as

$$\eta(i,j) = NA(i,j)/\sum_i \sum_j A(i,j), \quad (8)$$

where N is the total number of good (i,j) cells.

3.3. *Efficiency ratio of the area detector and M_1 monitor*

Information on the wavelength distribution of neutrons is required for the proper normalization of $S(q)$, as this array obtains contributions from a number of wavelength channels [see (7)]. Because the cryogenic moderator is the virtual source and a liquid-nitrogen-cooled MgO filter is in the beam, it is possible that the temperatures of these may drift during the long measurement times. This may alter the average spectral distribution of the neutrons for a given measurement. To determine the correct spectral distribution for a given experiment, the only information needed is the ratio of integrated intensity at the area detector to that at the M_1 monitor as a function of time channel (efficiency ratio). This is obtained by measurement of the intensity of the direct beam attenuated with a cadmium mask (2 mm-thick cadmium disk filled with tiny holes) using the area detector $E(i,j,k)$ and the M_1 monitor. This mask is designed to attenuate the beam intensity to within the linear range of the detector without altering the spectral

character of the neutron beam. The relative efficiency ratio, $\xi(k)$, for the neutrons in each time slice (k) is determined using the integrated intensity over the cells (i,j) within a radius of 5 cm with respect to the beam center in the area detector and those in the kth time slice of the M_1 monitor using the relationship

$$\xi(k) = \Big[\sum_i \sum_j E(i,j,k)\Big]/M_1(k). \tag{9}$$

The correct effective spectral distribution of neutrons for a given experiment is determined by multiplication of the relative efficiency ratio (Fig. 8) by the integrated counts in the M_1 monitor for each time slice. This information is then used for the normalization of the $S(q)$ [(7)] data for each experiment.

3.4. *Transmission coefficients*

For proper normalization of the scattering data, the wavelength-dependent transmission coefficients of each sample are required. The transmission coefficient is defined as the ratio of the sample-attenuated neutron beam to that of the unattenuated beam. To determine the wavelength-dependent transmission coefficients, the M_2 monitor (see Fig. 1) is lowered into the beam and measurements are made using both the M_1 and M_2 monitors. The wavelength-dependent transmission coefficients ranging between zero and unity are determined using the following:

$$\begin{aligned} T_s(k) = {} & [M_{1o}(k)M_{2s}(k)/M_{1s}(k) \\ & - M_{1o}(k)M_{2c}(k)/M_{1c}(k)]/[M_{2o}(k) \\ & - M_{1o}(k)M_{2c}(k)/M_{1c}(k)], \end{aligned} \tag{10}$$

where the subscripts c, o and s denote the cadmium, empty-camera and sample measurements, respectively, and $M_1(k)$ and $M_2(k)$ indicate counts in the kth time channel for monitors M_1 and M_2, respectively. As an example, the wavelength-dependent transmission coefficient of a 1 mm water sample is shown in Fig. 9. The measured transmission coefficient of 0.539 at 4.75 Å agrees well with the transmission coefficient of 0.543 measured at ORNL, where neutrons with $\lambda = 4.75$ Å and $\Delta\lambda/\lambda = 0.05$ are used. $T(\lambda)$ is linear for the majority of samples but the nonlinearity in $T(\lambda)$ for a 1 mm water sample may be due to multiple scattering or inelastic effects (Rennie & Heenan, 1993; Ghosh & Rennie, 1990).

3.5. *Multiple Bragg-scattering channels*

While defects in solids such as crystalline metallic alloys are studied, it may not be possible to use the full available range of neutron wavelengths. These crystalline materials will produce Bragg scattering of neutrons whose wavelengths are below the Bragg cut-off, which is twice the maximum interplanar spacing in the material. Such Bragg-scattered neutrons are sometimes scattered twice (or more) into the region sampled by the area detector. When only a few time channels are affected, they can usually be eliminated while the data are corrected to obtain $S(q)$. However, when the grain sizes are small, this procedure is not valid, and data from all wavelength channels below the Bragg cut-off must be omitted, the net result being the restriction of data in the high-q region.

3.6. *Effect of delayed neutron fraction*

There is an additional effect not formally indicated in (7). The use of fissionable materials for the target results in a contribution from delayed neutrons, in addition to the prompt neutron pulses. These delayed neutrons, of all wavelengths and having the same spectral distribution as neutrons from the prompt pulse, are emitted uniformly over the full duty cycle. These cause significant effects on the shape of the scattering profile. The measured value for the fraction of delayed neutrons in the IPNS-C1 beamline is 2.83% of the total for the enriched uranium target, while it is 0.44% of the total flux for the depleted uranium target. This measurement

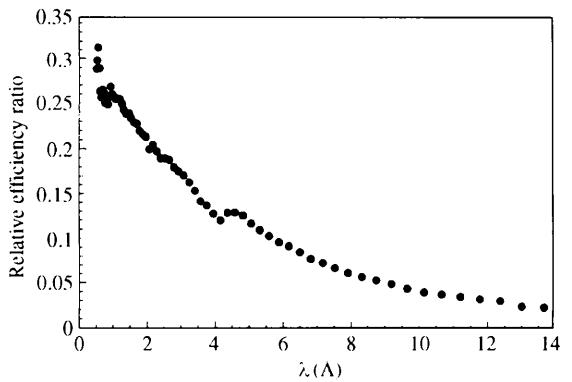

Fig. 8. The ratio of the integrated intensity at the area detector to that at the upstream monitor M_1 (relative efficiency ratio) as a function of wavelength at SAD.

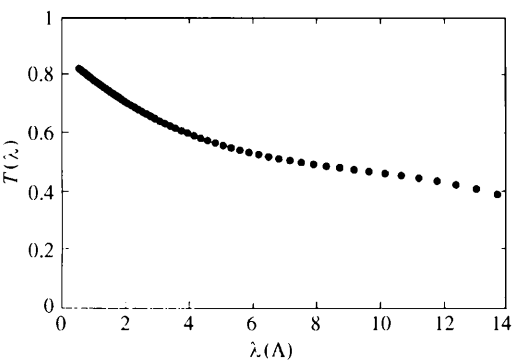

Fig. 9. Wavelength-dependent transmission coefficient of 1 mm H_2O measured at SAD.

and a method for correcting the various spectra for delayed neutrons have been reported (Epperson, Carpenter, Thiyagarajan & Heuser, 1990). The details of this procedure will not be repeated here but, to illustrate its importance when the IPNS enriched uranium target is used, we show the scattering data from SAD for one of our secondary intensity standards (Bates-poly), before and after correction for delayed neutrons, in Fig. 10. This figure also contains the correct absolute scattering cross section for this sample from the 30 m SANS instrument at ORNL (Bates & Wignall, 1986). The good agreement between the ORNL data and the corrected data from SAD shows the validity of our procedure to account for the effect of delayed neutrons. The delayed-neutron correction procedure is independent of the nature of the sample and hence is included in the data-reduction software. The data from M_1, M_2 and the area detector for every measurement must be corrected for delayed neutrons before the operations indicated by (7), (9) and (10) are carried out. The sharp decrease in $I(q)$ in the low-q region of the uncorrected data is actually due to the overestimation of the spectral intensity distribution in the long-wavelength region of the prompt neutrons.

4. Resolution

In the steady-state SANS instruments using a narrowly defined wavelength band of 'monochromatic' neutrons (typically, $\Delta\lambda/\lambda = 5-25\%$), the accessible q range depends on the geometry and the wavelength, and the resolution Δq is approximately constant for a given configuration. However, the Δq values vary for different instrument settings used for measuring the data in a wide q range. Owing to the different instrumental smearing, these scattering curves do not overlap and smearing effects have to be included in the analysis (Pedersen, 1993; Barker & Pedersen, 1995). In the data analysis for TOF-SANS instruments, neutrons initially binned into (i, j, k) position-wavelength cells are combined into q bins [see (4)]. Thus, the data in a given q bin come from a number of different (i, j, k) cells, each of which may have different q resolution determined by the time-of-flight resolution $\Delta t/t$ used in the data acquisition, the available solid angle of detection in the (i, j, k) cell and the incident-beam collimation. The final q resolution is a weighted average of the resolutions of the contributing (i, j, k) cells. When desired, resolution constraints can be imposed on the selection of (i, j, k) cells to be combined. The binning strategies used during data acquisition and data reduction will influence the resolution in the final q and the statistical precision of the intensity values (Hjelm, 1987, 1988).

In general, the resolution broadening in SANS instruments is determined by the geometric effects of collimation and the size of the detector element, and the wavelength dispersion used in the data acquisition. The relative contributions to the broadening width add in quadrature for a given wavelength and scattering angle as given below.

$$(\Delta q/q)^2 = (\Delta\theta/\theta)^2 + (\Delta\lambda/\lambda)^2. \qquad (11)$$

The resolution contribution from the pulse width for the decoupled solid methane moderator for SAD is very small ($\Delta\lambda/\lambda \simeq 0.01$) when compared with the size of the wavelength bins ($\Delta\lambda/\lambda = 0.05$) used at SAD. The geometric contributions to the resolution are independent of wavelength but depend on the scattering angle and can be calculated either analytically or by Monte Carlo methods (Carpenter & Faber, 1978; Mildner & Carpenter, 1984, 1987; Mildner, Carpenter & Worcester, 1986; Seeger & Pynn, 1986). Mildner & Carpenter (1987) have derived expressions for the geometrical resolution broadening in scalar q and vector q for instruments with Soller collimators. Hjelm (1987) has developed a method of calculating the r.m.s. deviation of the broadening distribution, $\sigma(q)$, for the TOF-SANS instruments, by including contributions from the geometrical and the TOF parameters. We calculated the $\sigma(q)$ values in the whole q range of SAD using this procedure. Fig. 11 shows $\sigma(q)$ as a function of q for two sizes of area detector on SAD when all available (i, j, k)

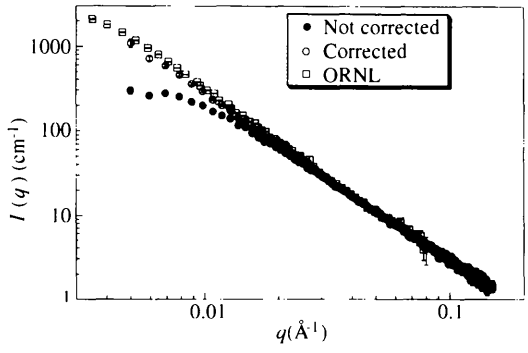

Fig. 10. Scattering from the Bates-poly sample illustrating the significance of the correction for delayed neutrons. The uncorrected data bend over in the low-q region.

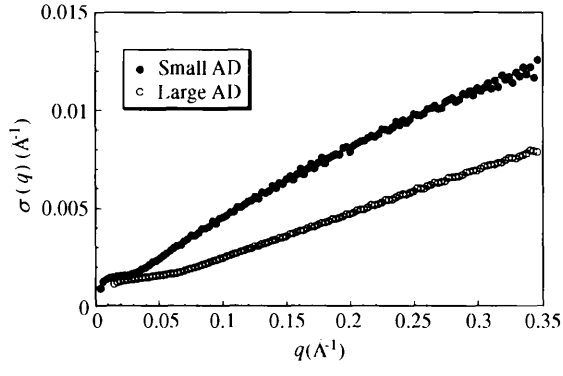

Fig. 11. The r.m.s. deviation of the broadening distributin $\sigma(q)$ as a function of q for the SAD. Data for a larger area detector correspond to 23 cm radius, when all cells contribute.

cells contribute. It can be seen that when a large detector is used on SAD, the q resolution will improve in the whole q region. The least effect in the very-low-q region is due to the fact that only a few cells corresponding to the smallest angle and the longest wavelength contribute to this region. The resolution calculations have been verified using the Bragg peaks of collagen (Mildner, *et al.*, 1986) and the crystalline phase of 17-hydroxy-3,6,9,12,15-pentaoxahexadecyl ethylene glycol monoester micelle in D_2O (Hjelm, 1988). One distinct advantage provided by the TOF-SANS instruments is that it is possible to improve the resolution in a given q region even after the experiment has been completed. This is accomplished by the proper selection of wavelength and area-detector cells as shown for 17-hy-droxy-3,6,9,12,15-pentaoxahexadecyl ethylene glycol monoester micelle in D_2O (Hjelm, 1988).

5. Absolute intensity calibration

The absolute differential scattering cross section is useful for determining parameters such as molecular weight, surface area, interaction parameters *etc.* (Wignall & Bates, 1987; Jacrot & Zaccai, 1981). The scale factor (F) for placing all the scattering data from SAD on an absolute scale is obtained by dividing the absolute scattering cross section of a standard sample typically measured at established SANS facilities by the scattering data measured at SAD. This scale factor combines all the normalization factors left out during the measurements of neutron spectral distribution, sensitivity of the area-detector pixels, wavelength-dependent efficiency ratios of the area detector and the M_1 monitor, and other instrumental effects. The conversion of the scattering from a given sample (thickness $= t$ cm) into absolute differential scattering cross section $I(q)$ in cm^{-1} sr^{-1} is carried out using:

$$I(q) = S(q)F/t \qquad (12)$$

6. Comparison of the performance of SAD with other established instruments

Despite the fact that the SANS instruments at the four pulsed-neutron sources, including IPNS, ISIS, LANSCE and KENS, have been operational for several years, the scientific community has not become fully familiar with these instruments. Even though neutron flux at a given wavelength is much smaller at IPNS than that at many reactor facilities, the large-wavelength band used in a time-of-flight mode at SAD actually compensates for such a shortcoming. In this paper, we use three examples to show that the quality of data and the measurement times at SAD are indeed comparable with the SANS instruments at other established centers in the world. Two more examples are used to illustrate the ease with which one can follow the phase behavior in a wide length scale by using SAD.

6.1. *Bates-poly*

The 'Bates-poly' is a polymer melt sample which consists of a 50:50 volume mixture of hydrogenous and perdeuterated high-molecular-weight polystyrene ($M_w = 1.15 \times 10^6$). Absolute SANS data for this sample were measured by Bates & Wignall (1986) at the steady-state neutron source (HFIR) at ORNL as well as our own measurement at the 30 m SANS instrument at ORNL and at the D11 measurement at ILL, France. Guinier analysis of the ORNL data measured with a sample-to-detector distance of 19 m gave $R_g = 334 \pm 3$ Å and $I(0) = 2804 \pm 28$ cm^{-1}. SAD cannot access the Guinier region of this sample. However, the scattering from this sample (Fig. 12) exhibits a q^{-2} power law in a wide high-q region and this has been very useful in placing the data from SAD on an absolute scale. The corrected data for this sample from SAD and the absolute scattering data measured either at D11 at ILL or those from the SANS instrument at ORNL are least-squares fitted in the region $0.035 < q < 0.055$ $Å^{-1}$ and the scale factor [F in (12)] is obtained by division of the absolute data by those from SAD. The excellent agreement between the data from SAD and those from D11 at ILL is shown in Fig. 12. The data from either ORNL or D11 at ILL were measured in two camera settings in order to cover the q range of 0.0035 to 0.08 $Å^{-1}$, whereas those from SAD span a much wider q range (0.005 to 0.35 $Å^{-1}$) in a single measurement. The total beam time used at D11 and ORNL at two camera settings were 300 and 450 s respectively, whereas the beam time at SAD was 1200 s to produce the data shown. However, the reconfiguration of the instrument and background measurements in the case of the reactor instruments require additional time. The statistical errors are similar in all these data sets in the region $0.01 < q < 0.08$ $Å^{-1}$. The fractional errors in the SAD data are small in this q range, but increase on

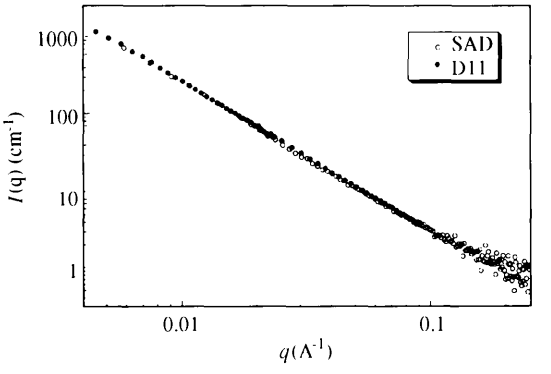

Fig. 12. Absolute scattering cross section of Bates-poly from SAD compared with the data from D11 at ILL, France. The ORNL data (not shown) agree well with these.

both sides of this q space. The quality of the data from SAD is thus comparable with the other established centers for SANS, moveover, with comparable measurement times.

6.2. *Silica gel*

A silica gel sample (packed powder in a 1 mm-thick Suprasil cell) whose scattering cross section remained constant during the past eight years also serves as a secondary intensity standard at SAD. The scattering data for this sample from the SANS instruments at ORNL and ILL yield $R_g = 44.9 \pm 0.5$ Å and $I(0) = 72 \pm 1$ cm^{-1} (Fig. 13). The SAD data for this sample scaled using the Bates-poly as a secondary standard provide $R_g = 45 \pm 0.9$ Å and $I(0) = 70 \pm 1.5$ cm^{-1}. Thus, the R_g and $I(0)$ values from SAD agree well with the data from D11 and the SANS instrument at ORNL. The measurement times for this sample are similar to those for the Bates-poly sample. The consistency in the value of the scale factor obtained from these two samples is often used to assess the performance of the instrument in terms of q calibration, absolute calibration, data rates *etc.*

6.3. *Vycor glass*

Another sample that has been used for the comparison of instruments is a vycor glass, which is a phase-separated system exhibiting a peak in its scattering. This sample has been measured at the pulsed-source-based SANS instrument LQD at LANSCE and at the reactor-based SANS instruments at D11 at ILL and that at the NG3 beamline at NIST (Hammounda, Krueger & Glinka, 1993), prior to the installation of the liquid-hydrogen moderator. We used two camera settings at D11 and a single setting at the SANS instrument at NIST. In Fig. 14, we show the data from SAD, LQD and the NG3 instrument at NIST. It is seen that the q corresponding to the peak as well as the intensity agree well (within 10%) in all the three measurements. The measurement took ~15 min at SAD ($0.005 < q < 0.35$ Å^{-1}) and LQD ($0.03 < q < 0.3$ Å^{-1}) while it took ~10 min at NIST using 8 Å neutrons with the detector at 6 m ($0.004 < q < 0.08$ Å^{-1}). The accessibility of a wide q region in a single measurement at SAD was very effective in the studies of the phase separation of a water–lutidine mixture in a confined geometry (Lin *et al.*, 1994) and the micellar formation and correlation in a porous medium (Bradley, Chen & Thiyagarajan, 1990), both of which used vycor glass as a medium.

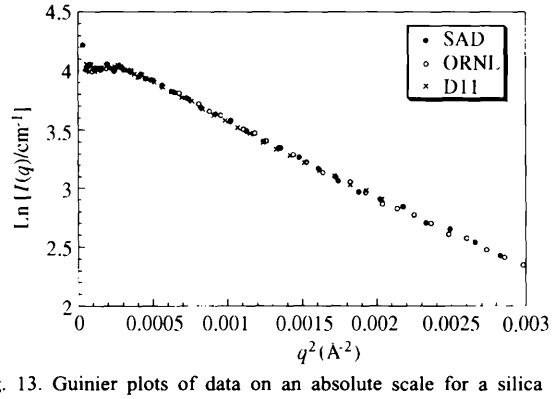

Fig. 13. Guinier plots of data on an absolute scale for a silica gel sample from SAD, 30 m SANS at ORNL and D11 at ILL, France.

7. Scientific examples

The advantage of SAD in producing data in a wide q region in a single measurement offers a unique opportunity for performing time-dependent studies. Two examples are given below to illustrate the ease with which one can explore the phase behavior by performing *in situ* SANS at SAD. It is important to point out that SAD will be very effective in the studies of systems under temperature, pressure or shear.

7.1. *Phase separation on graphite surface*

Binary mixtures of certain n-alkanes are known to undergo phase separation when quenched from the melt to ambient temperature. Owing to the high affinity of n-alkanes for the surface of graphite, the kinetics of phase separation of n-alkanes placed on a graphite are altered. To understand the phase separation of n-alkanes in the bulk and those on a graphite surface, Gilbert and coworkers have conducted extensive *in situ* SANS studies on alkanes of different chain lengths (Gilbert, Reynolds, Brown & White, 1996). The peaks corresponding to the phase-separating systems spanned a wide q range, so this experiment took advantage of the wide range in q available in a single run at SAD. Here we show the data for a sample consisting of a graphite substrate (compressed, exfoliated graphite, commercially available and known as 'papyex') into which is absorbed an equimolar

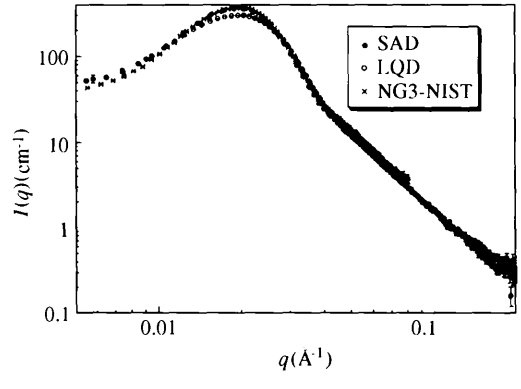

Fig. 14. Comparison of the absolute scattering cross section of a vycor glass sample measured at SAD, LQD and that measured at the SANS instrument on the NG3 beamline at NIST, prior to the installation of the liquid-hydrogen moderator.

mixture of two normal paraffins: n-$C_{30}D_{62}$ and n-$C_{36}H_{74}$. *In situ* SANS measurements were measured at 15 min intervals and the phase separation process was followed over one and a half days. Fig. 15 shows the time-resolved SANS data for a 1:4 mixture of $C_{30}H_{62}$:$C_{36}D_{74}$ doped into the porous graphite substrate quenched at 300 K. The major feature observed for the system is the presence of a diffuse peak at 0.12 $Å^{-1}$ ($d = 52.3$ Å) and progressive increase in the scattering in the region $q < 0.1$ $Å^{-1}$ with annealing time. The large intensity in the low-q region for the sample annealed for 15 min is from the graphite/alkane interface owing to the large contrast between the alkane mixture in the larger cavities of the graphite and the graphite substrate.

When isotropic substitution is employed in the binary alkane system resulting in a 4:1 mixture of $C_{30}D_{62}$:$C_{36}H_{74}$ doped into graphite, significantly different features are observed in the scattering (Fig. 16). Three peaks evolve at $q = 0.04$, 0.14 and 0.28 $Å^{-1}$. The first diffuse peak is due to the microphase separation, while the latter two are the first- and second-order peaks corresponding to a repeat distance of ~ 45 Å. The peaks of these mixed solid solutions are due to a (002) repeat in the orthorhombic form. This feature is seen to occur for $C_{30}H_{62}$:$C_{36}D_{74}$ at all quenching temperatures, and in all molar compositions studied, with no observable change in position with time.

The wide q range available in a single measurement at SAD (0.005 to 0.35 $Å^{-1}$) made each of the above time-dependent experiments easy to perform on a single sample. It would have been very difficult to perform these experiments at the reactor-based instruments as it would have involved several different samples (which may not be identical) measured at several reconfigurations of the instrument.

7.2. *Temperature- and pressure-dependent phase behavior of model biomembranes*

Aqueous dispersions of phosphatidylcholines provide valuable models for the investigation of biochemical and biophysical properties of biomembranes. These exhibit two temperature-dependent phase transitions, corresponding to lamellar gel-to-gel and gel-to-liquid crystalline phases at higher temperatures. In the liquid-crystalline phase, the hydrocarbon chains of the lipid are conformationally disordered, but the average chain orientation is perpendicular to the bilayer surface. In the gel phases, the chains are more extended and ordered; however, the lipid molecules can differ in bilayer surface structure and lipid chain packing. In the case of DPPC (1,2-dipalmitoyl-sn-glycero-3-phosphocholine), it has been shown that the gel phase has a two-dimensional lattice in which the lipid bilayers are distorted by a periodic ripple in the plane of the lamellae, whereas the lamellar gel phase has a plane bilayer surface while its hydrocarbon chains are tilted by $\sim 30°$ and packed in a distorted hexagonal lattice structure.

The structural properties of a number of saturated and unsaturated phosphatidylcholine model biomembranes under various temperatures and pressures were investigated using SANS (Winter & Thiyagarajan, 1990). Fig. 17 shows an example SANS of multilamellar saturated phospholipid DPPC vesicles in D_2O at 336 K as a function of pressure. This experiment also required a wide range in q as the peaks shift in q space as the

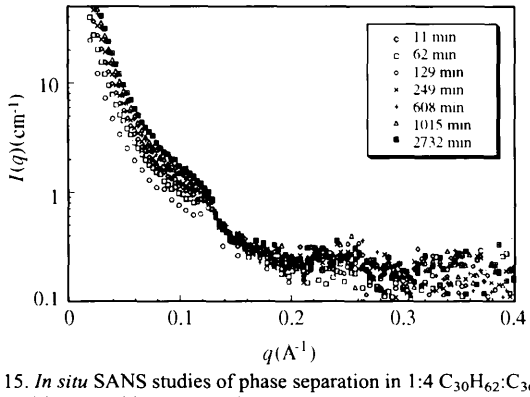

Fig. 15. *In situ* SANS studies of phase separation in 1:4 $C_{30}H_{62}$:$C_{36}D_{74}$ doped into graphite quenched at 300 K.

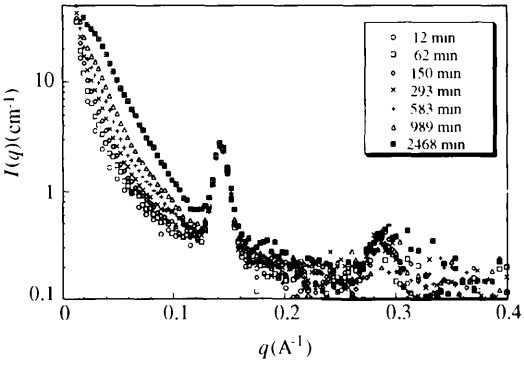

Fig. 16. *In situ* SANS studies of phase separation in 4:1 $C_{30}D_{62}$:$C_{36}H_{74}$ doped into graphite quenched at 300 K.

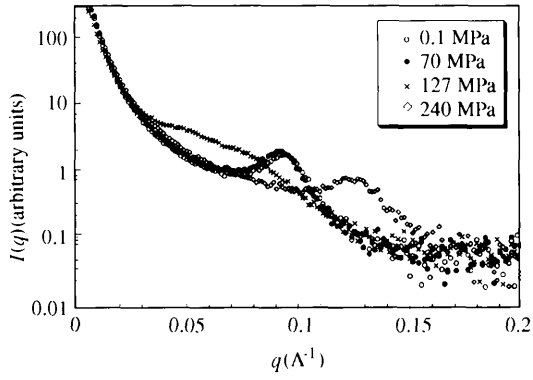

Fig. 17. SANS of DPPC undergoing phase transition as a function of pressure at 336 K.

temperatures and pressures were varied. At ambient pressure, DPPC exhibits a first-order diffraction peak corresponding to a d-spacing of 66 Å. This relates to the size of the repeat unit consisting of the bilayer and water layers around the head group. At 70 MPa the d spacing increases to 67.5 Å. Above 87 MPa (data not shown) the Bragg peak disappears and a transition from the liquid phase to the gel phase occurs, thus showing that increasing the pressure increases the liquid crystalline-to-gel phase transition temperature ($T_m = 315$ K at 1 bar). At 127 MPa the diffraction peak becomes diffuse showing the disorder in the system. At pressures above 179 MPa another diffraction peak develops (data not shown), which corresponds to a d spacing of 50 Å. The second high-pressure gel phase persisting even at 240 MPa is attributed to the interdigitation of the hydrocarbons in the bilayer.

8. Concluding remarks

Being a national user facility, the SAD at IPNS has served a wide spectrum of national and international users during the past decades [see the publication lists in Rotella (1991) and Marzec (1996) as well as earlier IPNS Progress Reports]. The wide q range accessible in a single measurement has been very effective in a number of studies on the shape of the particles, fractal dimension, polydispersity, aggregation, phase separation *etc.* as all these require fitting of the data in a wide q region. There is excellent agreement between the data from SAD and the steady-state SANS instruments at the established SANS facilities at ILL, ORNL and NIST. The results on the phase separation of n-alkanes by Gilbert *et al.* (1996) were derived from the data from both SAD and LOQ (Heenan & King, 1993), thus validating their similarity in quality and data rates. By using a vycor glass sample, we have shown that the data from SAD and LQD agree quite well. SAD was quite effective for the studies of the structure and polydispersity in the asphaltenes solution in deuterated n-methylnaphthalene at temperatures up to 673 K (Thiyagarajan, Hunt, Winans, Anderson & Miller, 1995). Since the TOF instruments are fixed geometry, additional detector banks can easily be added to increase both statistical precision and Δq resolution in a wide q region. For data in the middle q region (0.02 to 0.08 $Å^{-1}$), the q resolution in both types of instruments are comparable, but, at present, the steady-state instruments provide data of resolution superior to SAD in the very low q region. Matching of the performance of the TOF-SANS instruments with the best steady-state instruments in the low-q region is well within reach by the use of a combination of long-wavelength neutrons from cryogenic moderators, tighter collimation and detectors with better resolution.

Work was performed at the Intense Pulsed Neutron Source at Argonne National Laboratory, which is funded by the Office of Basic Energy Sciences, US Department of Energy, under contract number W-31-109-ENG-38. The authors acknowledge Elliot Gilbert and Professor John White, Australian National University, Canberra, Australia, for permitting us to use the SAD data on the microphase separation of paraffins.

References

Barker, J. G. & Pedersen, J. S. (1995). *J. Appl. Cryst.* **28**, 105–114.

Bates, F. S. & Wignall, G. D. (1986). *Macromolecules*, **19**, 934.

Borowski, C. J. & Kopp, M. K. (1975). *Rev. Sci. Instrum.* **46**, 951–962.

Bradley, K. F., Chen, S.-H. & Thiyagarajan, P. (1990). *Phys. Rev. A*, **42**, 6015–6023.

Carlile, C. J., Hey, P. D. & Williams, W. G. (1977). *J. Phys. E*, **10**, 543–546.

Carlile, C. J., Penfold, J. & Williams, W. G. (1978). *J. Phys. E*, **11**, 837–838.

Carpenter, J. M. (1987). *Nature (London)*, **330**, 358–360.

Carpenter, J. M. & Faber, J. (1978). *J. Appl. Cryst.* **11**, 464–465.

Carpenter, J. M., Mildner, D. F. R., Cudrnak, S. S. & Hilleke, R. O. (1989). *Nucl. Instrum. Methods*, A**278**, 397–401.

Carpenter, J. M., Walter, U. & Mildner, D. F. R. (1986). ICANS-IX. *Proceedings of the Ninth Meeting of the International Colaboration on Advanced Neutron Sources*, pp. 279–303. Report ISBN 3-907998-01-4. Schweizerisches Institut für Nuklearforschuntg, Switzerland.

Carpenter, J. M. & Yelon, W. B. (1986). In *Neutron Scattering*, edited by K. Skold & D. L. Price. *Methods of Experimental Physics*, Vol. 23, Part A, pp. 99–196. New York: Academic Press.

Chen, S.-H. (1986). *Ann. Rev. Phys. Chem.* **37**, 351–399.

Cotton, J. P. & Teixiera, J. (1986). *Physica B*, **136**, 103–105.

Crawford, R. K., Daly, R. T., Haumann, J. R., Hitterman, R. L., Morgan, C. B., Ostrowski, G. E. & Worlton, T. G. (1981). *IEEE Trans. Nucl. Sci.* NS-**28**, 3692–3700.

Crawford, R. K., Epperson, J. E. & Thiyagarajan, P. (1989). ICANS X. *Proceedings of the Tenth Meeting of the International Collaboration on Advanced Neutron Sources*, pp. 419–426. Los Alamos, NM, USA.

Crawford, R. K., Thiyagarajan, P. & Chen, J. (1994). ICANS XII. *Proceedings of the Twelfth Meeting of the International Collaboration on Advanced Neutron Sources*, pp. I208–215. Abingdon, Oxfordshire, England.

Epperson, J. E., Carpenter, J. M., Thiyagarajan, P. & Heuser, B. (1990). *Nucl. Instrum. Methods*, A**289**, 30–34.

Felcher, G. P., Hilleke, R. O., Crawford, R. K., Haumann, J., Kleb, R. & Ostrowski, G. (1987). *Rev. Sci. Instrum.* **58**, 609–619.

Ghosh, R. E. & Rennie, A. R. (1990). *Inst. Phys. Conf. Ser.* **107**, 233–244.

Gilbert, E. P. Reynolds, P. A., Brown, A. S. & White, J. W. (1996). *Chem. Phys. Lett.* **255**, 373–377.

Guinier, A. & Fournet, G. (1955). *Small-Angle Scattering of X-rays*. New York: Wiley.

Hammouda, B., Krueger, S. & Glinka, C. J. (1993). *NIST J. Res.* **98**, 31–46.

Haumann, J. R. & Crawford, R. K. (1987). *IEEE Trans. Nucl. Sci.* NS-**34**, 948–953.

Haumann, J. R., Daly, R. T., Worlton, T. G. & Crawford, R. K. (1982). *IEEE Trans. Nucl. Sci.* NS-**29**, 62–66.

Heenan, R. K. & King, S. M. (1993). *Proceedings of the International Seminar on Structural Investigations at Pulsed Neutron Sources, Dubna*. pp. 176–184. United Institute for Nuclear Research, Dubna.

Hjelm, R. P. Jr (1987). *J. Appl. Cryst.* **20**, 273–279.

Hjelm, R. P. Jr (1988). *J. Appl. Cryst.* **21**, 618–628.

Ibel, K. (1976). *J. Appl. Cryst.* **9**, 296–309.

Ishikawa, Y., Furusaka, M., Nimura, N., Arai, M. & Hasegawa, K. (1986). *J. Appl. Cryst.* **19**, 229–242.

Jacrot, B. (1976). *Rep. Prog. Phys.* **39**, 911–953.

Jacrot, B. & Zaccai, G. (1981). *Biopolymers*, **20**, 2413–2426.

Koehler, W. C. (1986). *Physica (Utrecht)*, **137**B, 320–329.

Kostorz, G. (1979). *Treatise on Materials Science and Technology*, Vol. 15, edited by G. Kostorz, pp. 227–289, New York: Academic Press.

Lin, M. Y., Sinha, S. K., Drake, J. M., Wu, X. L., Thiyagarajan, P. & Stanley, H. B. (1994). *Phys. Rev. Lett.* **72**, 2207–2210.

Lynch, F. J. (1980). *IEEE Trans. Nucl. Sci.* NS-**27**, 327–328.

Marzec, B. (1996). Editor. 15th Anniversary IPNS Progress Report. Vol. 1, pp. 32–45; Vol. II, 191–256. IPNS, Argonne National Laboratory, IL, USA.

Mildner, D. F. R. & Carpenter, J. M. (1984). *J. Appl. Cryst.* **17**, 249–256.

Mildner, D. F. R. & Carpenter, J. M. (1987). *J. Appl. Cryst.* **20**, 419–424.

Mildner, D. F. R., Carpenter, J. M. & Worcester, D. L. (1986). *J. Appl. Cryst.* **19**, 311–319.

Nunes, A. C. (1974). *Nucl. Instrum. Methods*, **119**, 291–293.

Nunes, A. C. (1978). *J. Appl. Cryst.* **11**, 460–464.

Ostanevich, Y. M. (1988). *Makromol. Chem. Macromol. Symp.* **15**, 91–103.

Pedersen, J. S. (1993). *Eur. Biophys. J.* **22**, 79–95.

Rotella, F. (1991). Editor. 10th Anniversary IPNS Progress Report, pp. 76–85; 161–163. IPNS, Argonne National Laboratory, IL, USA.

Rennie, A. r. & Heenan, R. K. (1993). *Proceedings of the International Seminar on Structural Investigations of Pulsed Neutron Sources*, pp. 254–260. United Institute for Nuclear Research, Dubna.

Seeger, P. A., Hjelm, R. P. Jr & Nutter, M. J. (1990). *Mol. Cryst. Liq. Cryst.* **18**A, 101–117.

Seeger, P. A. & Pynn, R. (1986). *Nucl. Instrum. Methods*, A**245**, 115–124.

Thiyagarajan, P., Bradley, K. F., Crawford, R. K., Epperson, J. E., Wozniak, D. G. & Carpenter, J. M. (1992). *Proc. Soc. Photo-Opt. Instrum. Eng.* **1737**, 243–254.

Thiyagarjan, P., Hunt, E., Winans, R. E., Anderson, K. B. & Miller, J. T. (1995). *Energy Fuels*, **9**, 829–833.

Wignall, G. D. (1987). *Encycl. Polym. Sci. Eng.* **10**, 112–184.

Wignall, G. D. & Bates, F. S. (1987). *J. Appl. Cryst.* **20**, 28–40.

Winter, R. & Thiyagarajan, P. (1990). *Prog. Colloid Polym. Sci.* **81**, 216–221.